Evaporation from a large lowland reservoir – (dis)agreement between evaporation methods at various timescales

Femke A. Jansen[1] and Adriaan J. Teuling[1]

[1]Hydrology and Quantitative Water Management Group, Wageningen University, Wageningen, The Netherlands

Correspondence: Femke Jansen (femke.jansen@wur.nl)

Abstract. Accurate monitoring and prediction of surface evaporation becomes more crucial for adequate water management in a changing climate. Given the distinct differences between characteristics of a land surface and a water body, evaporation from water bodies require a different parameterization in hydrological models. Here we compare six commonly used evaporation methods that are sensitive to different drivers of evaporation, brought about by a different choice of parameterization. We
5   characterize the (dis)agreement between the methods at various temporal scales ranging from hourly to 10-yearly periods, and we evaluate how this reflects in differences in simulated water losses through evaporation of lake IJsselmeer in The Netherlands. At smaller timescales the methods correlate less (r=0.72) than at larger timescales (r=0.97). The disagreement at the hourly timescale results in distinct diurnal cycles of simulated evaporation for each method. Although the methods agree more at larger timescales (i.e. yearly and 10-yearly), there are still large differences in the projected evaporation trends, showing a positive
10   trend to a more (i.e. Penman, De Bruin-Keijman, Makkink and Hargreaves) or lesser extent (i.e. Granger-Hedstrom and FLake). The resulting discrepancy between the methods in simulated water losses of the IJsselmeer region due to evaporation is ranging from -4 mm (Granger-Hedstrom) to -94 mm (Penman) between the methods. This difference emphasizes the importance and consequence of the evaporation method selection for water managers in their decision making.

1   Introduction

15   Surface evaporation is the second largest component (after precipitation) of the global hydrological cycle and it couples the Earth's water and energy cycle (Beer et al., 2018). This hydrological cycle is projected to intensify in the future as a consequence of global warming (Huntington, 2006; Oki and Kanae, 2006; Jung et al., 2010). This intensification will result in higher and more extreme precipitation and enhanced surface evaporation, which can threaten our drinking water resources and enlarge the vulnerability of natural ecosystems and agricultural production (Arnell, 1999; Vörösmarty, 2000; Middelkoop et al., 2001;
20   Verburg and Hecky, 2009; Trenberth et al., 2014). To avoid or alleviate negative consequences of droughts and floods, and to guarantee ample access to high quality fresh water resources, an efficient water management system is required. In a changing climate, the ability to accurately monitor and predict surface evaporation therefore becomes even more crucial for adequate water management, which is particularly essential in densely populated and hydrologically sensitive areas such as the low-lying Netherlands.

The Netherlands is an example of a region for which many studies have been dedicated to a better understanding of the processes driving the terrestrial part of surface evaporation including forested, agricultural and urban areas (de Bruin and Lablans, 1998; Dolman et al., 1998; Elbers et al., 2010; Vermeulen et al., 2015; Teuling, 2018). Resulting from the differences in surface characteristics, the dynamics of surface evaporation, as well as its sensitivity to different atmospheric drivers, will differ

5   over various land use types. For forests, Moors (2012) found that surface evaporation is mainly driven by the vapour pressure deficit (VPD). In contrast, surface evaporation over grasslands is typically driven by available energy through radiation, with little to no sensitivity to VPD (Makkink, 1957). This direct relation between net radiation and surface evaporation was also found by Beljaars and Bosveld (1997) for the grassland area around Cabauw, The Netherlands. For urban areas, Jacobs et al. (2015) found a clear negative relation between observed surface evaporation and days since the last precipitation event. This

10 can be attributed to the almost immediate drying of the fast impermeable surfaces, suggesting urban environments are strongly water-limited. In case of open water bodies wind speed was found to be the most important driver of evaporation according to Granger and Hedstrom (2011). Despite the fact that water bodies comprise a large share of the total area in The Netherlands (∼17%, (Huisman, 1998)) and therefore form a crucial element in our water management system, in the past only few studies in The Netherlands have focussed on open water evaporation (Keijman and Koopmans, 1973; de Bruin and Keijman, 1979;

15 Abdelrady et al., 2016; Solcerova et al., 2019).

During a short measurement campaign in Aug/Sept 1967 the vertical gradients of vapour pressure and temperature were measured at the water surface, and at 2 and 4 m above former Lake Flevomeer (Wieringa, 2019). It is assumed that the sign of these gradients can be used as a proxy for the sign of the turbulent exchange between the surface and the atmosphere. This proxy is used because there are no direct measurements available of E_{water} during the 1967 measurement campaign. To analyse

20 the difference between turbulent exchange above land surface and open water the observations of this measurement campaign above Flevomeer were compared to observations conducted above a grassland in Cabauw. The results show distinct differences despite the similar behaviour of global radiation, which is generally regarded as the main driver of evaporation. It demonstrates that both the temperature and vapour pressure gradients above the lake are positive throughout most of the day and night. This refers to unstable situations which become strongest during the night when the air cools faster than the water surface. The

25 continuous positive gradient of vapour pressure above the lake indicates that evaporation continues during the night, which is in contrast to what is found above land. Another distinct difference between land and lake surfaces can be found in the timing of the peak of the temperature and vapour pressure gradients, which are a few hours earlier above land than over the lake. From this experiment it directly becomes clear that we can distinguish a difference in behaviour of the turbulent exchange above land compared to over a lake, which therefore should be acknowledged in hydrological models.

30 Water surfaces have different surface properties than land surfaces which leads to a difference in behaviour of the turbulent exchange. One important difference is that solar radiation is able to penetrate a water surface, in contrast to a land surface which is not transparent. Therefore the energy balance is not preserved at the water surface, which entails heat storage in the water body. As a consequence of this thermal inertia, it was found that on shorter timescales the turbulent fluxes are not directly coupled to global radiation, and that the diurnal cycle of turbulent fluxes is smaller (Kleidon and Renner, 2017) and

35 shifted in time compared to land surfaces (Venäläinen et al., 1999; Blanken et al., 2011). Blanken et al. (2000) found, similar to
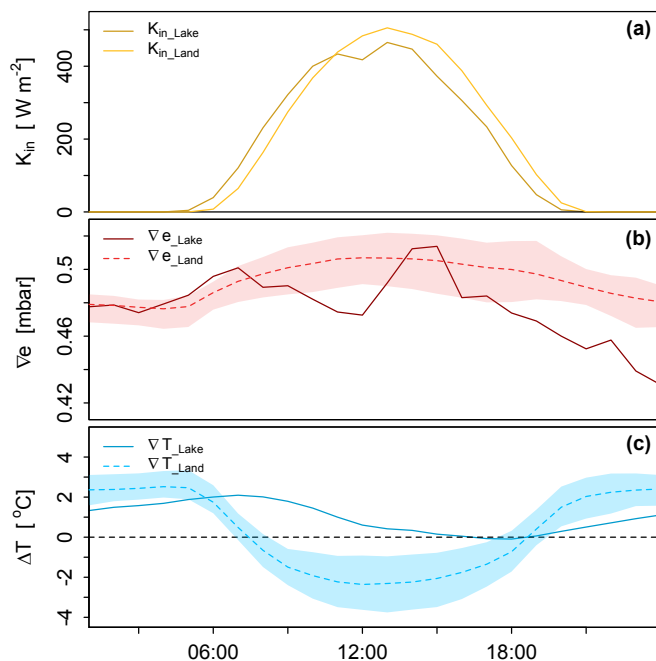
Figure 1. Illustration of the difference in behaviour of turbulent exchange above land compared to open water. Lake data is obtained above lake Flevomeer during the Flevo experiment in Aug/Sept 1967. Data above land originates from observations in Cabauw, and is based on ten Aug/Sept months of consecutive years (2009–2018); the solid line represents the average and the shaded bands represent the range in these ten years. The top panel presents the diurnal cycle of global radiation (**a**). The middle and bottom panel display the vertical gradients of vapour pressure and temperature for the lake and land surface (**b** and **c**, respectively).

Granger and Hedstrom (2011), a relation between evaporation and the product of horizontal wind and vapour pressure gradient on daily timescales. In contrast, Nordbo et al. (2011) found the vapour pressure deficit alone to be more strongly correlated to evaporation rather than the product of wind and vapour pressure deficit. On intraseasonal timescales, Lenters et al. (2005) found evaporation to be a function of the thermal lag between temperatures of air and water. Resulting from the difference in

5   properties and consequently its behaviour, the simulation of evaporation from lakes requires a different parameterization than land surface evaporation in current traditional hydrological models, and with that accounting for the relevant driving processes at the timescale of interest.

In hydrological modelling, surface evaporation is a key source of uncertainty when it comes to its short-term prediction and long-term projection. Depending on the parameterization strategy of a model to capture the process of evaporation at the

10   relevant timescale, different decisions are made to parameterize evaporation. In the past, most studies have focussed on the parameterization of open water evaporation on weekly or even longer timescales (Finch, 2001; Zhan et al., 2019), where often potential evapotranspiration (PET) is improperly used as a proxy for lake evaporation neglecting heat storage (La, 2015; Duan and Bastiaanssen, 2017). However, parameterization at the hourly and daily timescales have remained underexplored. Melsen

et al. (2018) recognized that through this parameterization, additional uncertainty is introduced to the model results. As a consequence, the effect of the parameterization strategy on the short-term prediction and long-term projection of evaporation can lead to profound differences in model results and therefore in (local) water management decisions. Our aim therefore is to study the effect of various parameterizations of evaporation on shorter-term local water management, and to investigate how

5 these parameterization decisions affect long-term hydrologic projections. To this end, we compare to what extent six commonly used evaporation parameterizations (dis)agree at various temporal scales, and look at the impact of the different methods under projected climate change.

2 Methods and data

2.1 Evaporation methods

10 There is a wide variety of methods that are used to estimate evaporation from water bodies. They can be subdivided into five major types of approach, namely the pan method, water balance method, energy budget approaches, bulk transfer models and combination methods (Finch and Calver, 2008; Abtew and Melesse, 2013). In this study, we will systematically compare six methods that are commonly used to estimate surface evaporation and that are sensitive to different forcings (Table 1, see Table A1(b) for the explanation of all variables).

15 The Penman method (Penman, 1948) has been chosen because it was originally developed for wet surfaces and because it is the most commonly used method globally to estimate evaporation. The method developed by de Bruin and Keijman (1979) finds its origin in Penman's method, but has been based on observations done at lake Flevomeer, The Netherlands, where we will focus on in this study as well (see Sect. 2.2). Makkink's method (Makkink, 1957) is an even more simplified derivation of Penman's equation and is currently used in operational hydrological models in The Netherlands, which is why it is included

20 in our comparison. To be able to compare it to methods that use other types of forcing, the methods of Granger and Hedstrom (2011), using wind speed as main forcing, and the Hargreaves (1975) method, using solely air temperature, are incorporated. To also include a more physical-based method, FLake (Mironov, 2008) is used in this study. Below we will give a short description of the models that are used, and in Appendix A a more detailed description is given of the methods, including the assumptions that are made, and the input data that is needed for them (see Table A1).

25 ### 2.1.1 Penman

The Penman method is a combination equation and it is based on the two fundamental factors that determine evaporation, namely: available energy and atmospheric demand (see Tab. 1). The effect of these factors combined is captured by the turbulent transfer and energy balance equations for a wet surface (Brutsaert, 1982; Tanny et al., 2008; Moene and van Dam, 2014).

Starting from the energy balance principle combined with the flux-gradient approach, the following form of Penman's equation is derived:

$$\lambda E = \frac{s}{s+\gamma}(R_n - G) + \frac{\frac{\rho c_p}{r_a}(e_{sat}(T) - e_a)}{s+\gamma}, \tag{1}$$

In Penman's derivation, it was assumed that the available energy (Q_n) is equal to the net radiation (R_n), assuming other terms
5 of the energy budget equation into the water body to be negligible, e.g. the water heat flux (G). This water heat flux is difficult to measure, especially at smaller timescales, and is therefore often ignored (van Emmerik et al., 2013). However, for water bodies it is essential to account for heat storage changes as its storage capacity is significantly larger compared to land surfaces. Not accounting for heat storage changes can lead to (i) overestimation of E_{water} in spring (Northern Hemisphere) when incoming radiation is used to warm up the water body instead of immediate release through E_{water}, and (ii) underestimation of E_{water}
10 during autumn (Northern Hemisphere) when additional heat that was stored in the water body is released through E_{water}. The Penman equation requires standard meteorological variables (net radiation, air temperature, wind speed and humidity) at one height.

2.1.2 De Bruin-Keijman

A similar expression to determine reference evaporation was proposed by de Bruin and Keijman (1979). They applied the
15 Priestley-Taylor method to former lake Flevomeer in The Netherlands. The Priestley-Taylor method is a derivation of Penman's method where the aerodynamic term in Penman's equation was found to be a constant proportion of the radiation term (Priestley and Taylor, 1972). de Bruin and Keijman (1979) adjusted this empirical relation to determine evaporation, namely that the aerodynamic term is linearly proportional to the radiation term with an additional constant added to that. These two parameters were found to vary during the year, but they are mostly taken as constants.

2.1.3 Makkink

20

Another method that is based on Priestley-Taylor is the method of Makkink, which was developed for grassland areas in summertime in The Netherlands (Makkink, 1957). It only requires observations of global radiation and temperature, since it assumes that the water heat flux can be neglected with respect to net radiation, and that net radiation is about half of global radiation. The first assumption is only valid for land surfaces, and the second assumption considers average summers in The
25 Netherlands. Makkink is currently used in operational hydrological models in The Netherlands and is applied to open water using a correction factor.

2.1.4 Granger-Hedstrom

None of the methods described above include wind explicitly, although wind speed is recognized to be an important driving factor for evaporation. Granger and Hedstrom (2011) found the most significant correlation to exist between E_{water} and wind
30 speed at hourly timescales, and no direct relation was found with net radiation. The authors developed a simple model to

quantify E_{water} in which the key variables and parameters are: wind speed, land-water contrasts in temperature and humidity, and downwind distance from the shore.

2.1.5 Hargreaves

The Hargreaves method is an example of a simple and highly-empirical temperature-based model (Hargreaves, 1975; Hargreaves and Allen, 2003). Global surface radiation is frequently not readily available, therefore the Hargreaves method uses the extra-terrestrial radiation, which depends on the angle between the direction of solar rays and the axis perpendicular to the atmosphere's surface, to simulate its seasonality. Furthermore it incorporates the range in maximum and minimum temperature as a proxy to estimate the level of cloudiness. The method has originally been designed for land surfaces at longer temporal scales and does not account for lake heat storage. However, previous studies have also shown that temperature-based model can perform reasonably well over lake surfaces at larger timescales (Rosenberry et al., 2007).

2.1.6 FLake

A more physical-oriented model is FLake which has been developed by Mironov (2008). This one-dimensional freshwater model is designed to simulate the vertical temperature structure and the energy budget of a lake. It consists of an upper mixed layer, of which the temperature is assumed to be uniform, and an underlying stratified layer of which the curve is parameterized using the concept of self-similarity (assumed-shape) (Kitaigorodskii and Miropolskii, 1970). The same concept is used to represent the thermal structure of the ice and snow cover and of the thermally active layer of the bottom sediments.

Table 1. Methods to calculate evaporation. Explanation of all variables can be found in Table A1(b).

| Method	Short description	Equation	Reference
Penman	Combines a radiation term and an aerodynamic term.	$\lambda E = \frac{s}{s+\gamma}Q_n + \frac{\gamma}{s+\gamma}E_a$	Penman (1948)
Makkink	Based on same principles as Priestley-Taylor using only temperature and global radiation	$\lambda E = 0.65 \frac{s}{s+\gamma}K_{in}$	Makkink (1957)
De Bruin - Keijman	Alternative to Penman's equation using data from Flevomeer experiments (1967).	$\lambda E = \alpha_{BK}\frac{s}{s+\gamma}(R_n - G) + \beta_{BK}$	De Bruin and Keijman (1979)
Granger & Hedstrom	A simple hourly E_{water} model using the relationship with wind.	$E = a*u$ $a = f(\Delta T, \Delta e, X)$	Granger and Hedstrom (2011)
Hargreaves	Temperature-based method	$ET_{ref} = 0.0023R_a(TC + 17.8)TR^{0.50}$	Hargreaves and Allen (2003)
FLake	A two-layer parametric fresh water model. Capable to predict the vertical temperature structure.	$\lambda E = -(q_z - q_s)\frac{u_* k}{Sc_n}\frac{L_v \rho}{(ln(\frac{z}{z_0}) + \psi_q(z/L)}$	Mironov (2008)
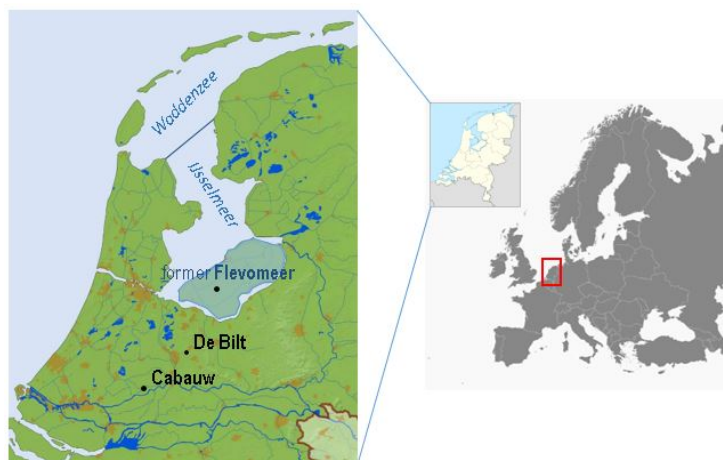
Figure 2. Overview of the area of interest and the locations of the observational stations used in this study.

2.2 Study area

This research study focusses on lake IJsselmeer, which is the largest fresh water lake in The Netherlands, bordering the provinces of Flevoland, Friesland, and Noord-Holland. In the north IJsselmeer is closed off from the Waddenzee by the Afsluitdijk embankment and in the southwest by the Houtribdijk embankment. The lake receives its fresh water supply ($\sim$340 m^{3}s^{-1}) from the river IJssel and from the neighbouring polder systems, whereas the main outflow of the lake occurs at the sluices of the Afsluitdijk under gravity. Covering an area of 1100 km^2 with an average depth of 5.5 m, the IJsselmeer can be considered a large shallow lake. The lake has an important hydrological function in the low-lying Netherlands both in flood prevention and fresh water supply for agricultural and drinking water purposes.

2.3 Data input sources

The models were forced with observed historical hourly data (1960–2018), as well as with simulated 3-hourly future climate projections (2019 – 2100) resulting from a regional climate model (RCM). In this study we systematically compare the models; therefore, we chose to give preference to a long-term dataset of observed meteorological variables above land, rather than a shorter-term dataset of the same variables in more close proximity to lake IJsselmeer. Following from this, we used the long-term hourly meteorological data observed in De Bilt, The Netherlands, situated at approximately 50 km distance. Depending on the required data for each model (see Table A1), this includes air temperature (T_{air}), global radiation (K_{in}), air pressure (P), wind speed (u), wind direction, relative humidity (RH) and cloud cover. Furthermore, water surface temperature (WST) is required as a variable in the Granger-Hedstrom model, as well as to calculate outgoing longwave radiation. WST is not operationally measured at a regular base in The Netherlands, however the Dutch water authority (RWS) measures hourly water temperature at a depth of about 1 meter in the IJsselmeer since 2014. Another source of WST measurements is an experiment done in 1967 (Keijman and Koopmans, 1973; Wieringa, 2019) in former lake Flevomeer before that part of lake IJsselmeer

was reclaimed. This experiment includes four weeks of data of amongst others WST, average water temperature, and T_{air} and vapour pressure at 2 and 4 m height. Furthermore, FLake generates WST simulations as well. Remotely sensed satellite products inferring WST were not considered because of its low temporal resolution, but will be used in upcoming studies to infer the spatio-temporal distribution of E_{water}. Comparing the different sources (not shown) and considering the availability of

5 the data, it has been chosen to use the FLake simulations of WST for further analysis.

To quantify the (dis)agreement between the models on the long-term projection of E_{water}, we used climate projections generated with the RCM RACMO2 (van Meijgaard et al., 2008) driven by the global climate model (GCM) EC-EARTH 2.3 (Hazeleger et al., 2012). This long-term simulation covers the period 1950 – 2100 and consists of 16 ensemble members at a spatial resolution of $0.11°$ (~ 12 km) available at 3-hourly timesteps (Aalbers et al., 2017). Each member of the ensemble has

10 a slightly different atmospheric initial state perturbed in 1850, and the members can thus be considered as independent realizations. EC-EARTH was forced with historical emissions until 2005 and future projections (2006 – 2100) were generated using a substantial greenhouse gas emission scenario (RCP8.5). We used a grid cell representing location De Bilt. Direct evaporation observations from an eddy-covariance instrument at 10-min time resolution made in Cabauw, The Netherlands, from 1986 – 2018 (Beljaars and Bosveld, 1997) are used to validate the climate change signal of E and its sign.

15 ## 2.4 Diurnal cycle

Methods that are sensitive to different types of forcings show a distinct diurnal signal of simulated evaporation. A wide variety of evaporation methods use K_{in} as a driving force to simulate the diurnal cycle of evaporation, partly because K_{in} affects temperature, vapour pressure deficit (VPD) and wind speed, which are all driving forces of evaporation. Therefore, an analysis of the diurnal signals and possible phase shift of these variables provide information on how these driving forces relate to each

20 other and to the simulated evaporation.

We depict the diurnal cycle as function of time for one specific day where no clouds were present, as well as for the average diurnal cycle for the period 1960 – 2018 using data from De Bilt, The Netherlands (see Fig. 2 and Section 2.3). Another way that we will use to analyse and illustrate the diurnal cycle and the relation to other evaporation methods, is to plot evaporation as a function of K_{in} similar to Renner et al. (2018). When this cycle appears as a hysteresis loop, it indicates a phase difference

25 between the addressed variable and K_{in}. The size of the loop quantifies the magnitude of the phase lag, and the direction of the loop denotes if the phase lag is negative or positive. The method of Hargreaves will be omitted in these diurnal cycle analyses. This method requires a temperature maximum and minimum (see Appendix A) over the considered time period. Therefore, it is not possible to calculate hourly simulated evaporation for this method with the given hourly observations of temperature.

2.5 Long-term trends

30 To explore how evaporation has been changing in the last decades (1960 – 2018) and how it is projected to change in the future (2019 – 2100) in a changing climate, we will force the methods with historical observations and simulated future projections of meteorological variables resulting from the regional climate model RACMO, using a grid cell representing De Bilt (Section 2.3). The trend of the yearly averaged simulated evaporation rates will be detected based on weighted local regression, using the

LOcally WEighted Scatter-plot Smoother (LOWESS) method (Cleveland, 1979). This method is applied to the observational data for the historical period, and to the average of the 16 RACMO members (Section 2.3) for the future period. Mean and standard deviation are calculated using the average of the RACMO members, where the standard deviation is calculated based on the de-trended time series.

2.6   Model (dis)agreement

A difference in sensitivity of the methods to drivers of evaporation can help to explain the (dis)agreement found in behaviour of simulated evaporation. To compare this sensitivity a perturbation of 1% will be imposed one by one on the daily observational data from De Bilt of four key variables, namely air temperature, solar radiation, wind speed and vapour pressure, without changing the other variables. For this, the percentage difference of simulated evaporation with perturbation of one of the variables, to the simulation of the baseline situation without any perturbation, will be calculated.

The correlations between the simulated evaporation using the different methods and various meteorological variables using data from De Bilt will be calculated based on Pearson's parametric correlation method, measuring the linear dependency between two variables. We will calculate the correlations for all the timescales ranging from hourly to 10-yearly period all based on hourly data. To ensure that the number of data points in the calculation is not influencing the results, we will apply bootstrapping to artificially create the same number of data points for each timescale.

3   Results and discussion

3.1   Simulation of the diurnal cycle

The diurnal signal of several meteorological variables and simulated evaporation are depicted in figure 3. The solid lines are the results from a sunny day without any clouds in March 2016, while the dotted lines reflect the average diurnal cycles. It can be seen that net radiation (R_n) peaks between 1pm and 2pm, which coincides with the peaks of evaporation simulated using the radiation-based methods, i.e. Penman (PN), de Bruin-Keijman (BK) and Makkink (MK). Evaporation becomes negative during the night following net radiation in case of the first two methods. However, this is not realistic given the fact that the energy balance is not preserved at the water surface, which is assumed by these methods, and the energy released from heat stored in the water can exceed the net radiation at night. This will drive both a positive evaporation and sensible heat flux. Evaporation simulated with the wind-driven Granger-Hedstrom (GH) method is damped relative to the radiation-based methods, and it is rather constant throughout the day, with a small peak following the signal of the wind speed. The signal of evaporation resulting from FLake (FL) is damped as well, and its peak is lagging 2 hours behind relative to R_n, induced by a combination of K_{in}, wind speed and T_{air}. The total average diurnal evaporation is significantly lower than for the radiation-based methods. This can be explained by the remaining heat storage term of the energy balance in FL, which is used to warm up the water. This heat storage capacity is explicitly accounted for in FL. Hargreaves' temperature-based method (HA) is not depicted in the graph because the method does not allow to calculate evaporation at hourly timescales given the available data (see Sect. 2.4). The
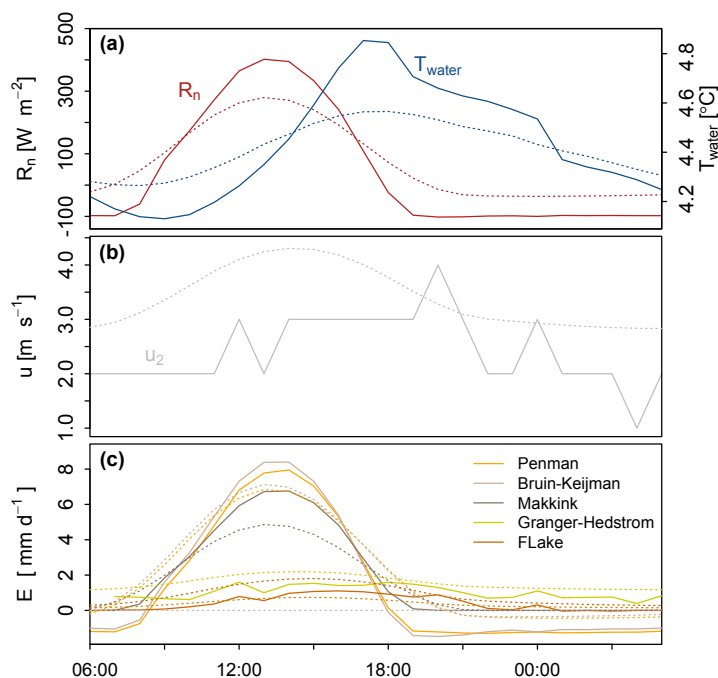
Figure 3. Illustration of the diurnal response of simulated evaporation using different methods (**c**) in relation to several types of meteorological forcing (**a** and **b**). Solid lines represent a sunny day in March 2016, while the dotted lines indicate the average diurnal cycle based on the years 1960 – 2018.

diurnal range of the water temperature (T_{water}) is small, but shows a distinct peak four hours lagging behind the peak of R_n, which indicates that during the day heat is stored in the water, which partly is released back during the night. The dotted line illustrating the average diurnal cycle of T_{water} was artificially lowered by 7.5 degrees Celcius in this graph, merely to show its diurnal course and the timing of the peak.

5

Figure 4 illustrates the diurnal cycle of the (a) latent heat flux, (b) vapour pressure, and (c) temperature, which are plotted as a function of K_{in} for a sunny day without any clouds in March 2007. It can be seen that evaporation simulated using the MK method is almost in phase with K_{in} (phase lag is 7 min), which may be expected from a method that uses K_{in} as the main driving force of evaporation. The largest phase lag (=114 min) results from the simulation with FL; this can be explained by

10   the fact that this method explicitly accounts for heat storage changes, resulting in a less direct response of evaporation to K_{in}. The analysis of diurnal patterns thus shows that K_{in} explains most of the variance in evaporation for the methods PN, BK and MK. However, the methods that incorporate heat storage capacity and/or WST as an explaining variable show less variation in evaporation during the day and therefore do not relate directly to K_{in}.

Air temperature has a distinct counter-clockwise (CCW) loop which indicates that heat is stored in the lower part of the

15   atmospheric boundary layer (ABL). However, the water surface temperature shows very little response to K_{in}. This combination
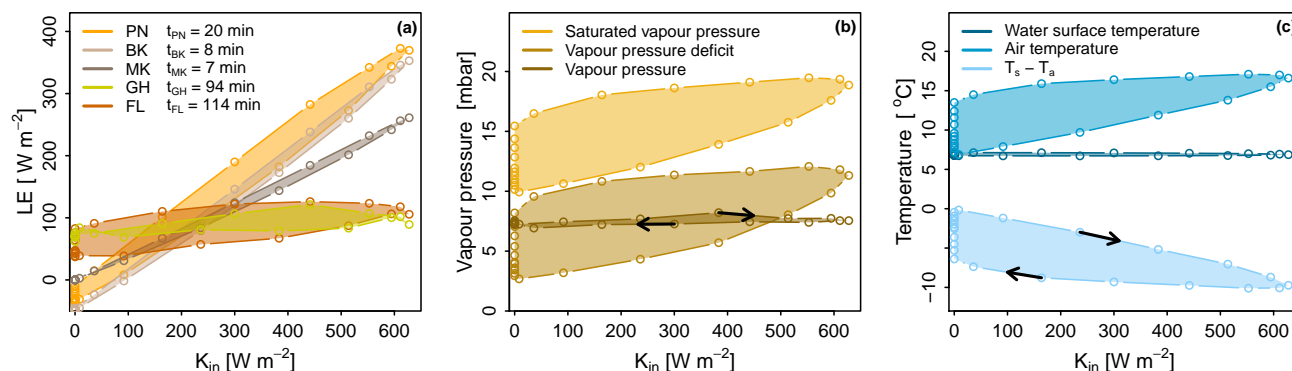
Figure 4. Phase difference of simulated evaporation to global radiation (**a**), and of different components of vapour pressure and temperature to global radiation (**b** and **c**, respectively) for a day in March 2007. In the legend the daily phase lag in minutes is displayed. The direction of all hysteresis loops are counter-clockwise, indicating a positive phase lag with respect to global radiation, except for the two loops that have a clockwise direction indicated by a black arrow.

leads to another distinct hysteresis loop of the driving force of sensible heat flux, namely the gradient T_s-T_a, which has a clockwise (CW) direction. This implies that the latent heat flux is preceded by the sensible heat flux. The vapour pressure is rather constant throughout the day and does not display a clear hysteresis loop. However, the saturated vapour pressure, which is a function of T_{air} displays pronounced CCW hysteresis. As a result, VPD also has a large CCW hysteresis loop, which is the key driver of E in the PN method.

Following the analyses of the diurnal cycle the occurence of storage and release of heat in the water body is demonstrated through the diurnal cycle of T_{water}, and should therefore be accounted for by an evaporation method. FL is the method that mimics this thermal inertia effect most clearly in its diurnal cycle, which is also supported through its phase lag to K_{in}. This makes the FL method the most realistic method to use at this timescale.

3.2 Long-term simulations and projections

For each method the simulated evaporation rates based on either observations in De Bilt or on RACMO realizations, are shown in Fig. 5 for the historical (1960 – 2018) and future (2019 – 2100) period (note that the values on the y-axes differ). The grey lines indicate the 16 realizations of the RCM RACMO members, while the black line is the simulation resulting from

observational data measured in De Bilt. The dotted blue line represents the trend of this black line. Following the positive trend of evaporation as was observed in Cabauw (red line in the lowest panel), all methods, except for the GH method, also simulate a positive trend in the historical time period when using observations from De Bilt (black line). Apart from methods GH, HA and FL, the RACMO realizations resulting from the RCM simulations also show positive trends in the historical

5   period. However, these trends are not as strong as the trends resulting from the simulations which use observations from De Bilt. For the future period these RACMO realizations have a stronger positive trend compared to the historical period for all methods, again except for GH and FL. This implies that the RACMO simulations do not always agree with the simulations which are based on observations; however, they do demonstrate the differences between the six methods regarding predicted future trends.

10 The results from the GH and FL method differ from the other methods in the sense that the RACMO realizations do not result in a significant trend in either the simulated historical or the projected future period, while in the historical period the simulation based on observations presents a positive trend when using the FL method. The latter can be explained by the fact that the FL method is most sensitive to K_{in}, T_{air} and wind speed, of which for both K_{in} and wind speed the RACMO realizations do not show any trend (not shown here). The mismatch in the historical period for FL between the simulation based on observations

15 and the simulations based on RACMO realizations can be attributed to the inability of RACMO to capture the trend in K_{in}. This inability will also influence the simulations made by the radiation-based models, which implies that for these methods simulated trends in the future period are likely to be stronger than demonstrated in figure 5. This will lead to even larger disagreement of simulated evaporation between the six methods.

Comparison between the methods of the overall positive trend that is projected to continue in the future period, reveals that

20 not only the average simulated evaporation of all RACMO members (μ) will increase in the future for all the methods, ranging from an increase of 0.02 mm d^{-1} (GH and FL) to 0.24 mm d^{-1} (PN), but also that the variability (σ) is projected to increase (see Fig. 5). This is also demonstrated in figure 6 for both the historical (orange) and future (blue) period. Here the spread is defined as the difference between the yearly average maximum and minimum value of the 16 RACMO members based on daily evaporation rates. For each method the average and the spread is projected to increase in the future, however, the rates at which

25 this happens differ significantly between the methods. The largest difference in spread can be found between the GH method, which has a spread of 0.32 mm d^{-1}, and PN method with a spread of 0.69 mm d^{-1} in the historical period, and increases to a range that varies from 0.36 mm d^{-1} (GH) to 0.94 mm d^{-1} (PN) in the future period. The methods that resemble each other most, and differ least in spread, are the PN and BK method during both the historical and future period.

3.3 Model (dis)agreement at various timescales

30 Figure 7 displays the difference in percentage of simulated evaporation with the baseline situation without any perturbation. The upper and lower set of panels depict the same information arranged per variable or per method, respectively. Most of the methods show the largest sensitivity to T_{air} and K_{in}. The purely temperature driven HA method is only sensitive T_{air}. The wind-driven GH method is the method most sensitive to wind (1% difference), which is expected, but FL also is sensitive to wind showing a difference of 0.5% compared to the baseline situation without any perturbation. This implies that the behaviour
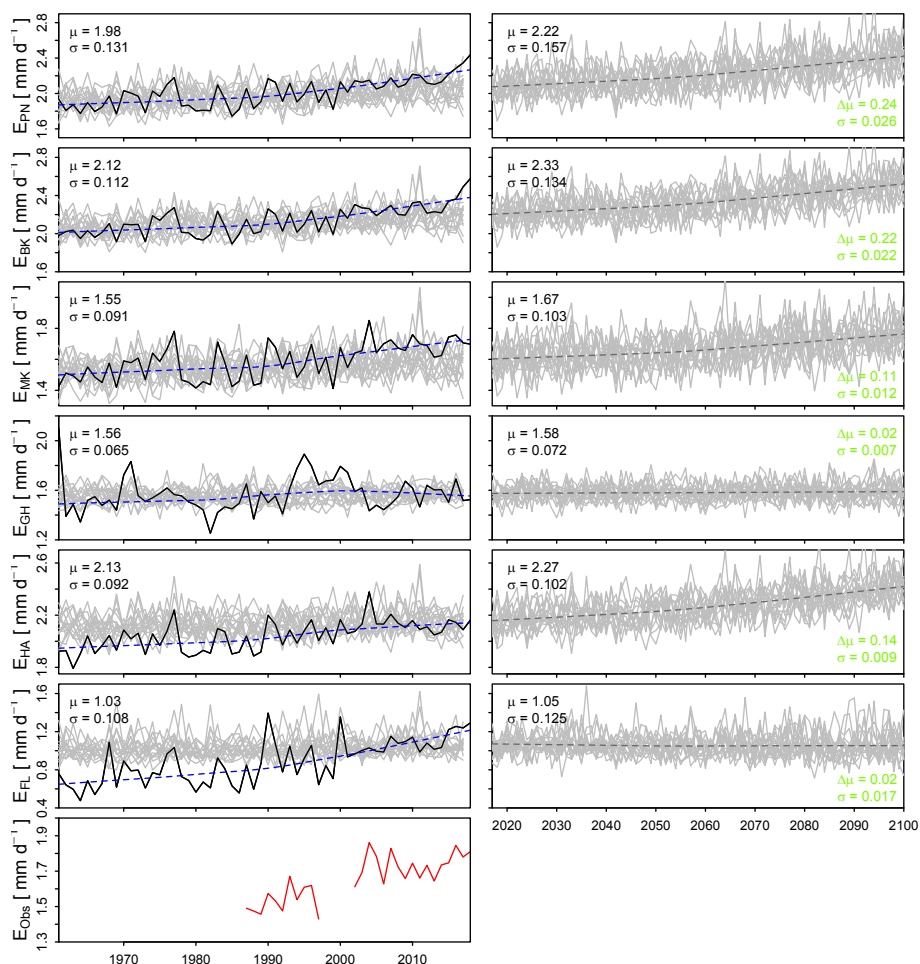
Hydrology and
Earth System
Sciences
Discussions
EGU
Open Access

Figure 5. Trends of simulated evaporation for the historical (1960 – 2018) and future (2019 – 2100) period based on RACMO realizations. Black line indicates yearly averaged simulated historical evaporation rates based on data from De Bilt. The dotted blue line represents the trend in this line. The gray lines indicate the yearly averaged simulations from RACMO climate projections. Mean and standard deviation of the RACMO simulations are given in each panel in black. The differences of these statistics between the historical and future period are given in green. In the lowest panel the yearly averaged observed evaporation at meteorological site Cabauw is presented in red.
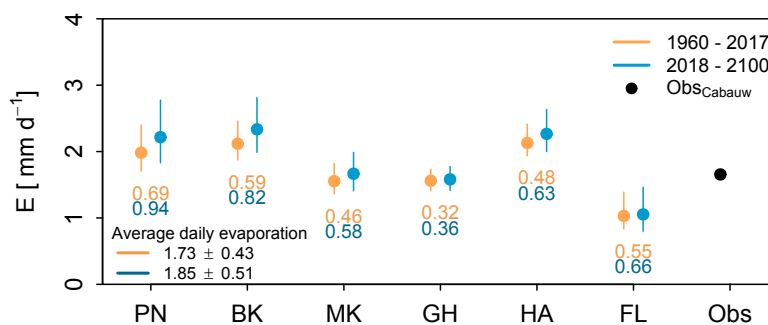
Figure 6. Projected change of the average and spread of simulated evaporation based on RACMO realizations. Coloured dots indicate the mean of all RACMO members for each method for both the historical and future period. Coloured numbers below each method indicate the spread within the method. Here spread within the methods is defined as the difference between the average maximum and minimum value of all RACMO members for both periods, based on yearly average daily evaporation rates (see Fig. 5). The black dot represents the averaged observed evaporation in Cabauw over the period 1986 – 2017.

of these models would start to deviate more from the other methods if for instance the wind speed regime were to change in the future. In general FL is the most sensitive method, and therefore this method will start to differentiate more from the other methods when these four meteorological variables were to change in the future.

Figure 8 displays to what extent the evaporation methods and four meteorological variables correlate at (a) hourly, (b) daily,
5   (c) weekly, (d) monthly, (e) yearly and (f) 10-yearly timescales based on data from De Bilt. The colours indicate the direction and magnitude of the correlations. From our data the HA method can only be calculated at a daily timescale or coarser, hence the empty boxes at the hourly timescale. It becomes apparent that at hourly timescales there is a positive correlation between wind and simulated E ranging from 0.12 for the MK method, to 0.84 for the GH method. At larger timescales, this correlation becomes negative, except for the wind-driven GH method, and for FL it remains positive until a daily timescale. At
10   the two largest timescales considered here (Fig. 8e and f) the correlation with wind increases again, but these are statistically insignificant except for the GH method. The correlation between net radiation and simulated E remains high at all timescales, except for the GH method. The latter method shows low correlations with the other methods and most meteorological variables, which mostly become statistically insignificant (indicated by the numbers in grey) from weekly timescales and larger. The correlation between net radiation and E simulated using FL increases steadily from 0.63 to 0.94 with increasing timescale.
15   Regarding the correlation between E and T_{air}, and E and VPD, the matrices show that the correlations increase steadily for all evaporation methods, again with the exception of the GH method. However, it should be noticed that there is a dip in the correlation at yearly timescales, which is clearly visible in Figure 9. Furthermore, the correlation between the meteorological variables R_n, T_{air} and VPD was found to increase with increasing timescale.

The radiation-based methods agree highly with each other, as can be expected, over the entire range of timescales, with
20   correlation values above 0.9. The GH method deviates most in terms of correlation from the other methods, which could be attributed to the difference in sensitivity to wind speed. The HA method shows the largest increase in agreement to the
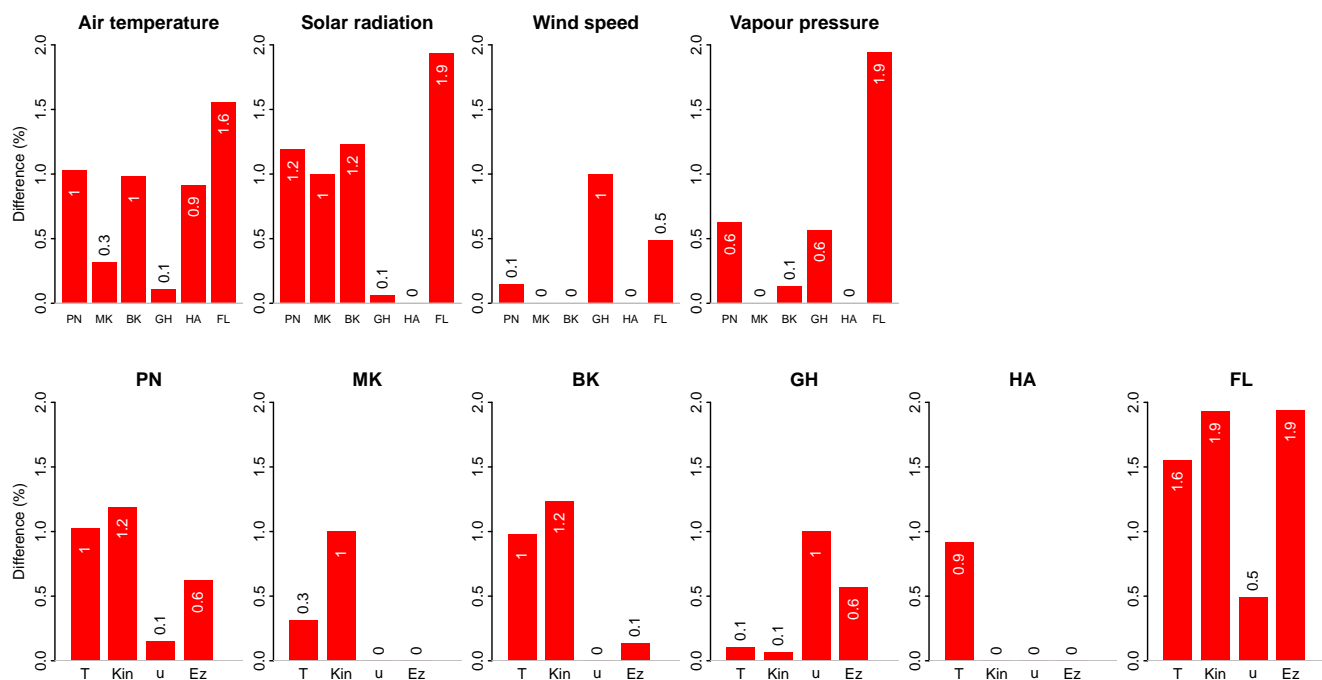
Figure 7. The effect of a systematic perturbation of several meteorological drivers on simulated evaporation. This effect is expressed as the percentual difference between the perturbed simulation and the baseline. Upper set of panels arranged per variable. Lower set of panels displays same information but clustered per method.

radiation-based methods with increasing timescale. This can be attributed to the increasing correlation between temperature and net radiation, which are the main driving forces of the HA and the radiation-based methods, respectively. Comparing the average correlations between the models for each timescale reveals that the correlation increases with increasing timescale from 0.72 at hourly to 0.97 at 10-yearly timescale. This increase implies that the methods on average tend to agree more with each

5   other at coarser timescales, which means that at smaller timescales the consequence of model choice becomes more apparent. The average correlation at the daily timescale is lowered mainly as a consequence of the low correlations of the GH method to the radiation-based methods. It should be noted that insignificant values were not incorporated in the calculation of the average correlations.

10   In Fig. 9 the correlation (r) between simulated evaporation and VPD, T_{air} and R_n respectively are depicted to further explore the (dis)agreement between the methods over the range of timescales. This correlation has been calculated based on observational data from De Bilt. In general there is a high correlation (r > 0.75) between simulated E and VPD, which is increasing with
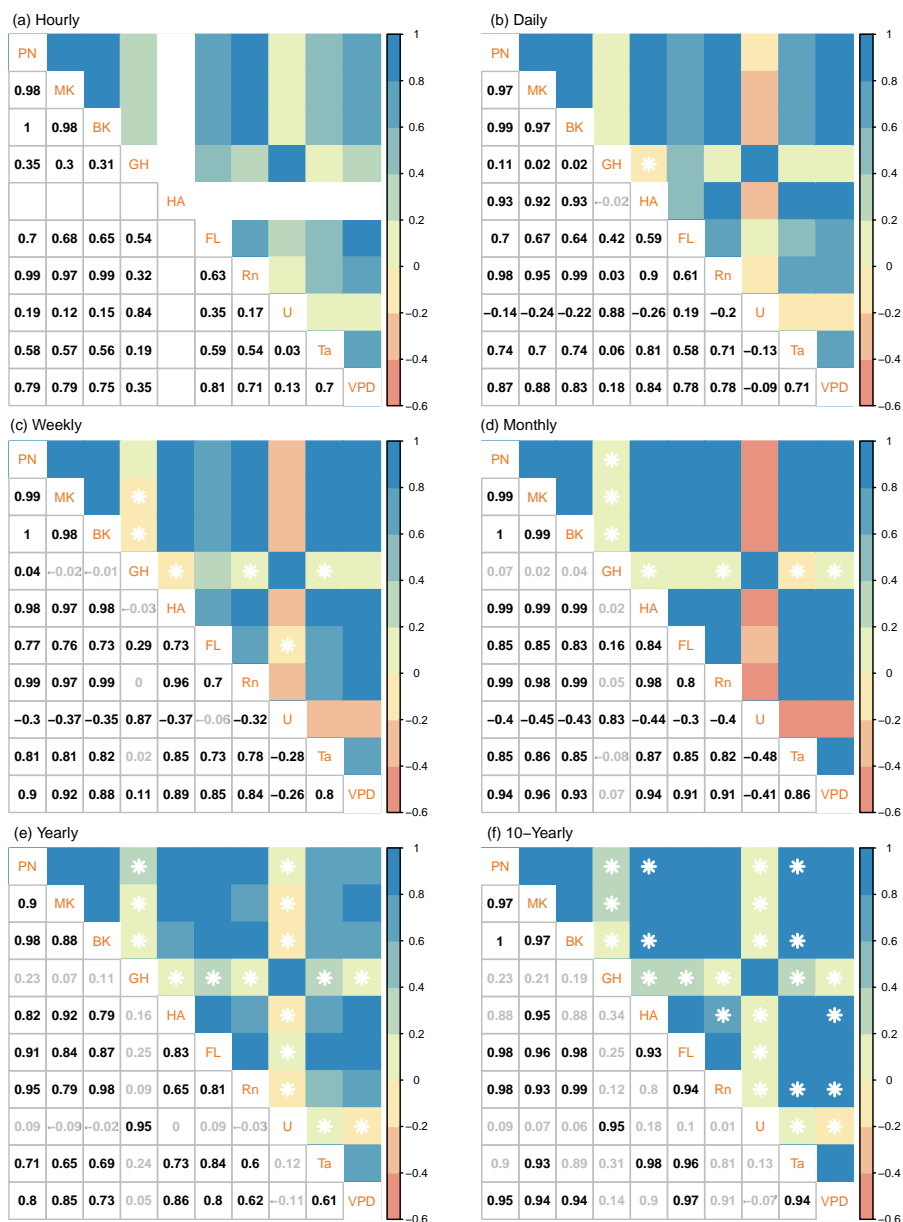
Figure 8. Correlation between simulated evaporation and meteorological variables at (**a**) hourly, (**b**) daily, (**c**) weekly, (**d**) monthly, (**e**) yearly and (**f**) 10-yearly timescale. The colours indicate the sign and strength of the correlation. A white star, and corresponding grey number, marks insignificant correlations ($\alpha = 0.01$).

Hydrology and
Earth System
Sciences
Discussions

Open Access

EGU

increasing timescales, up to correlations of 0.97 at the 10-yearly timescale. However, there is a small drop at the yearly timescale. We were not able to determine the exact cause of this, but it could be a result of cross-correlation in the data. The GH method deviates in behaviour compared to the other five methods, since it is the only method that does not explicitly include T_{air}, and with that VPD through the saturated vapour pressure, which is a function of temperature. The GH method

5 only includes a temperature gradient as additional information to wind speed. The correlation between simulated E and T_{air} increases from 0.57 at the hourly timescale up to 0.98 at the 10-yearly timescale, again with a small drop at the yearly timescale. Furthermore, similar to the correlation with VPD, the GH method again demonstrates a different behaviour compared to the other methods. There is a strong increase of the correlation at the yearly and 10-yearly timescale for this method, which could be related to a change of the sign to positive values for the correlation between wind speed and T_{air} at these timescales (see Fig.

10 8). The correlations to R_n demonstrate clearly the resemblance between the radiation-based methods PN, BK and MK. The HA method shows similar correlations as well, except for the largest two timescales where the correlation is lower. The FL method correlates better to R_n with increasing timescale, confirming that at small timescales R_n is not a direct driver of E as a result of heat storage. The correlation between R_n and E simulated by the GH method is close to zero for daily timescales and larger. However, at the hourly timescale the correlation is 0.32. This corresponds to the larger correlation between wind speed and R_n

15 at this timescale.

The general increase of the correlations with the meteorological variables that was found with increasing timescales, implies that ultimately these variables act as driving forces of potential evaporation. However, at the shorter timescales some of these methods may fail because the wrong controlling variables are used to simulate actual evaporation. This is especially the case for methods that use R_n as a driver of evaporation and that omit the effect of thermal inertia as a result of heat storage.

20 ## 3.4 Implications for water resources management

Table 2 presents for several years the water loss through evaporation expressed as water depths in mm for the IJsselmeer region. Meteorological data from De Bilt was used to force the evaporation methods in case of the two average years and the two dry years. For the years 2000 and 2100 projected evaporation was based on the 16 RACMO members. During average years the water level of the IJsselmeer would lower by 649 mm on average as a result of evaporation, if it would not be compensated

25 by incoming fluxes through precipitation and water supply by rivers. Large differences were found between the methods. The HA method and FL are at both ends of the spectrum, where HA simulates largest losses through evaporation (745 mm), while FL simulates less than half of that (310 mm) in 1986. During dry years the total water loss through evaporation increases to on average 677 mm, but within a specific year, e.g. 2003, it ranges from 868 mm using the HA method to 376 mm using FL to simulate evaporation. Due to the large differences of simulated evaporation between the various methods, the result of

30 the simulated water balance of the lake could be positive or negative. This means that based on the method used to simulate evaporation, the water managers would make different decisions on whether to stop the water inlet to the surrounding land for agricultural purposes or not for instance, or whether more or less water needs to be discharged to the Waddenzee to keep the level of the IJsselmeer region within a safe range. And because there are no direct operational measurements of evaporation
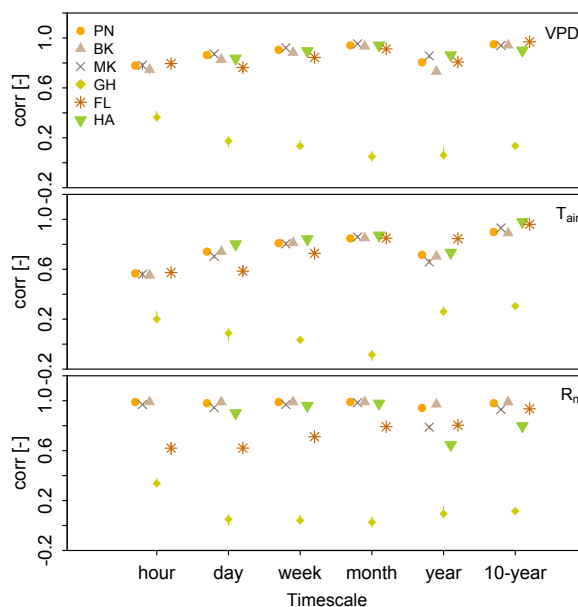
Figure 9. Correlation between simulated evaporation and VPD, T_{air} and R_n respectively over the range of timescales based on observational data.

available in the IJsselmeer region, this stresses even more that the knowledge of the discrepancy between the methods is of great importance for water managers in their decision making.

This discrepancy is projected to increase in the future when comparing the results based on the average of the RACMO realizations for the years 2000 and 2100. The radiation-based and temperature methods show a growing water loss through

5   evaporation, while for GH and FL the water loss remains similar. All methods show increasing evaporation rates leading to lower water availability in the region, where the change in mean water depth from the year 2000 to 2100 is ranging from -4 mm (GH) to -94 mm (PN). This means that when water managers would rely on the PN method rather than on the GH method for instance, they will have to decide for instance to supply less water to the surrouding land surfaces.

The effect of the projected changes of evaporation in the future was found to be largest in summer (Fig. 10), which coincides

10   with the period that has the highest evaporation rates. This summer period is therefore most critical regarding water resources management, also considering the fact that more extreme periods of drought are expected to occur more frequently. During summer, evaporation is thus projected to increase, and at the same time it is likely that with increasing temperatures the river discharge from the IJssel will decrease (Görgen et al., 2010). So less water will be available during summer, while the water demand from the surrounding land surfaces will increase for agricultural purposes. The trade-offs water managers have to make

15   therefore become very precarious, while knowing that the methods project significantly different results.

Table 2. Water losses through evaporation for the IJsselmeer region for average and dry years, and for a historical and future year. Water losses are expressed as water depths.

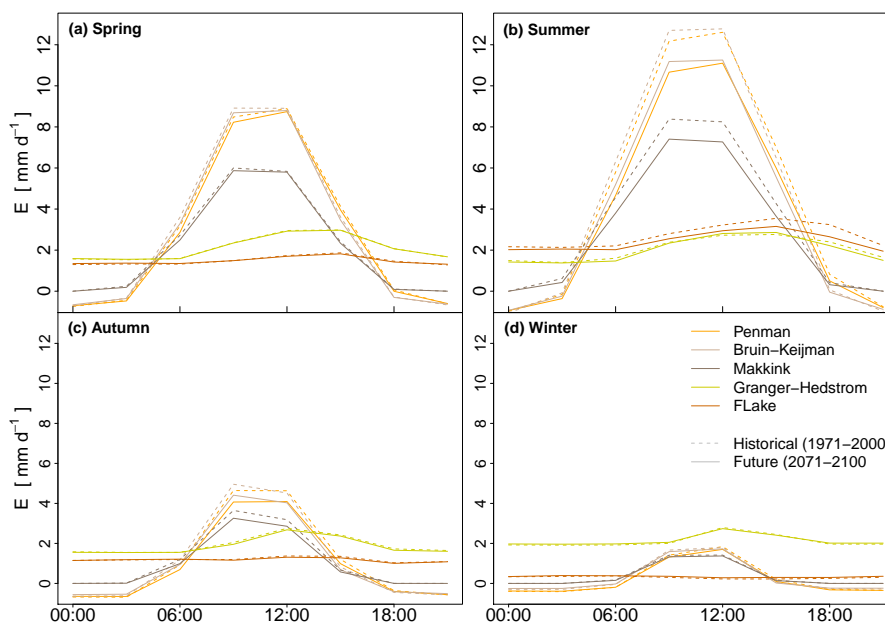| [mm]	Average year		Dry year		2000	2100	Δ Water depth
	1986	2009	1976	2003			2000 − 2100
Penman	678	781	760	761	733 ± 50	827 ± 62	-94 ± 80
De Bruin-Keijman	706	817	791	799	751 ± 41	830 ± 49	-79 ± 64
Makkink	594	642	652	676	591 ± 33	652 ± 39	-61 ± 51
Granger-Hedstrom	683	628	676	565	732 ± 32	736 ± 38	-4 ± 49
Hargreaves	745	788	819	868	677 ± 31	751 ± 33	-74 ± 45
FLake	310	417	378	376	503 ± 36	508 ± 50	-5 ± 62

Figure 10. Projected change of diurnal cycle of evaporation per season based on RACMO realizations. Solid lines represent the historical period and the dotted lines the future period. The simulations for the two average years and the two dry years were forced with observational data from De Bilt. For the years 2000 and 2100 projected evaporation was based on the 16 RACMO members.

4 Conclusions

The aim of this study was to explore the effect of various conceptualizations of evaporation on shorter-term local water management and long-term hydrologic projections. We focussed on timescales ranging from hourly to 10-yearly periods, where we have (i) elaborated on the differences found in the diurnal cycle, but also (ii) quantified the (dis)agreement between the methods over the range of timescales in terms of correlations. And moreover, we studied how the evaporation rates according to the various methods are projected to change in the future.

Our study characterized that there is a large effect of the type of forcing that is used by the evaporation method, especially on the simulated diurnal cycle. This difference is reflected in the total average daily evaporation, the timing of the evaporation peak and the day/night cycle. All radiation methods (PN, BK and MK) follow the diurnal cyle of the net radiation, where MK becomes zero at night, and PN and BK negative. The simulated evaporation resulting from the GH and FL methods are more constant throughout the day and on average they show a continuation of evaporation during the night. Data of T_{water} demonstrated heat storage during the day and release of heat during the night. FL is the method that mimics this effect of thermal inertia most clearly in its diurnal cycle. This makes the FL method the most realistic method to use at this timescale. At larger timescales we found a disagreement between the methods in the trend of yearly averaged daily evaporation rates both for the historical (1960 – 2018) and future period (2019 – 2100). Although both the average and the variability of all methods is projected to increase in the future, the rate at which this happens differs significantly between the methods. The average evaporation rate increase ranges from 0.02 mm d^{-1} (GH and FL) to 0.24 mm d^{-1} (PN).

A discrepancy at the whole range of evaluated timescales, from hourly to 10-yearly, is especially present between the radiation and temperature methods (PN, BK, MK and HA), and the wind driven (GH) and physical-based lake (FL) methods. However, this disagreement generally decreases with increasing timescale, which is to be expected considering that ultimately evaporation is constrained by the energy input in the system and the transport of water vapour. However, the difference at yearly timescales is still significant. This can be seen from the large differences found when translating the discrepancy of simulated evaporation into yearly water losses through evaporation for lake IJsselmeer. For an average year this can range between 417 mm (FL) and 817 mm (BK). During a sensitive dry year this discrepancy can result in water levels to be simulated to either rise or drop, solely depending on the evaporation method that is used. When considering future simulations, the projected change in mean water losses through evaporation, expressed as water depths, ranges from -4 mm (GH) to -94 mm (PN) when comparing the year 2000 to 2100. This means that when water managers would rely on the PN method rather than on the GH method, they might have to decide to supply less water to the surrounding land in the future. Therefore, owing to the disagreement between the methods, it reveals that the choice of method is of great importance for water managers in their decision making. To gain confidence in which method is most reliable to use, now and in the future, we suggest to perform long-term direct observations of E_{water} at high temporal resolution. This will help to improve optimal parameterization of E_{water} in hydrological models.

Hydrology and
Earth System
Sciences
Discussions
Open Access

EGU

Author contributions. FJ and AJT designed the study. FJ carried out the study, analyzed the data and wrote the manuscript. AJT contributed to the writing and the interpretation of the results.

Competing interests. The authors declare that they have no conflict of interest.

References

Aalbers, E. E., Lenderink, G., van Meijgaard, E., and van den Hurk, B. J. J. M.: Local-Scale Changes in Mean and Heavy Precipitation in Western Europe, Climate Change or Internal Variability?, Climate Dynamics, 50, 4745–4766, https://doi.org/10.1007/s00382-017-3901-9, 2017.

Abdelrady, A. R., Timmermans, J., Vekerdy, Z., and Salama, M. S.: Surface Energy Balance of Fresh and Saline Waters: AquaSEBS, Remote sensing, 8, 583, https://doi.org/10.3390/rs8070583, 2016.

Abtew, W. and Melesse, A. M.: Evaporation and Evapotranspiration: Measurements and Estimations, Springer Netherlands, 2013.

Arnell, N. W.: Climate Change and Global Water Resources, Global Environmental Change, 9, S31–S49, https://doi.org/10.1016/S0959-3780(99)00017-5, 1999.

Beer, T., Li, J., and Alverson, K.: Global Change and Future Earth: The Geoscience Perspective, Cambridge University Press, 2018.

Beljaars, A. C. M. and Bosveld, F. C.: Cabauw Data for the Validation of Land Surface Parameterization Schemes, Journal of Climate, 10, 1172–1193, https://doi.org/10.1175/1520-0442(1997)010<1172:CDFTVO>2.0.CO;2, 1997.

Blanken, P. D., Rouse, W. R., Culf, A. D., Spence, C., Boudreau, L. D., Jasper, J. N., Kochtubajda, B., Schertzer, W. M., Marsh, P., and Verseghy, D.: Eddy Covariance Measurements of Evaporation from Great Slave Lake, Northwest Territories, Canada, Water Resources Research, 36, 1069–1077, https://doi.org/10.1029/1999WR900338, 2000.

Blanken, P. D., Spence, C., Hedstrom, N., and Lenters, J. D.: Evaporation from Lake Superior: 1. Physical Controls and Processes, Journal of Great Lakes Research, 37, 707–716, https://doi.org/10.1016/j.jglr.2011.08.009, 2011.

Brutsaert, W.: Evaporation into the Atmosphere: Theory, History and Applications, Springer Netherlands, 1982.

Cleveland, W. S.: Robust Locally Weighted Regression and Smoothing Scatterplots, https://doi.org/10.1080/01621459.1979.10481038, 1979.

de Bruin, H. A. R. and Keijman, J. Q.: The Priestley-Taylor Evaporation Model Applied to a Large Shallow Lake in The Netherlands, Journal of Applied Meteorology, 18, 898–903, 1979.

de Bruin, H. A. R. and Lablans, W. N.: Reference Crop Evapotranspiration Determined with a Modified Makkink Equation, Hydrological Processes, 12, 1053–1062, https://doi.org/10.1002/(SICI)1099-1085(19980615)12:7<1053::AID-HYP639>3.0.CO;2-E, 1998.

Dolman, A. J., Moors, E. J., Elbers, J. A., and Snijders, W.: Evaporation and Surface Conductance of Three Temperate Forests in the Netherlands, Annales des sciences forestières, 55, 255–270, 1998.

Duan, Z. and Bastiaanssen, W. G. M.: Evaluation of Three Energy Balance-Based Evaporation Models for Estimating Monthly Evaporation for Five Lakes Using Derived Heat Storage Changes from a Hysteresis Model, Environmental Research Letters, 12, 024 005, https://doi.org/10.1088/1748-9326/aa568e, 2017.

Elbers, J., Moors, E., and Jacobs, C.: Gemeten Actuele Verdamping Voor Twaalf Locaties in Nederland, 2010.

Finch, J. and Calver, A.: Methods for the Quantification of Evaporation from Lakes, World Meteorological Organisation's Commission for Hydrology, 2008.

Finch, J. W.: A Comparison between Measured and Modelled Open Water Evaporation from a Reservoir in South-East England, Hydrological Processes, 15, 2771–2778, https://doi.org/10.1002/hyp.267, 2001.

Görgen, K., Beersma, J., Brahmer, G., Buiteveld, H., Carambia, M., de Keizer, O., Krahe, P., Nilson, E., Lammersen, R., Perrin, C., and Volken, D.: Assessment of Climate Change Impacts on Discharge in the Rhine River Basin: Results of the RheinBlick2050 Project, no. 23 in CHR Report 1, Secretariat CHR/KHR, Lelystad, oCLC: 698494614, 2010.

Granger, R. J. and Hedstrom, N.: Modelling Hourly Rates of Evaporation from Small Lakes, Hydrology and Earth System Sciences, 15, 267–277, https://doi.org/10.5194/hess-15-267-2011, 2011.

Hargreaves, G. H.: Moisture Availability and Crop Production, Transactions of the ASAE, 18, 0980–0984, https://doi.org/10.13031/2013.36722, 1975.

5 Hargreaves, G. H. and Allen, R. G.: History and Evaluation of Hargreaves Evapotranspiration Equation, Journal of Irrigation and Drainage Engineering, 129, 53–63, https://doi.org/10.1061/(ASCE)0733-9437(2003)129:1(53), 2003.

Hazeleger, W., Wang, X., Severijns, C., Ştefănescu, S., Bintanja, R., Sterl, A., Wyser, K., Semmler, T., Yang, S., van den Hurk, B., van Noije, T., van der Linden, E., and van der Wiel, K.: EC-Earth V2.2: Description and Validation of a New Seamless Earth System Prediction Model, Climate Dynamics, 39, 2611–2629, https://doi.org/10.1007/s00382-011-1228-5, 2012.

10 Huisman, P.: Water in the Netherlands, no. 3 in NHV-Special, Netherlands Institute of Applied Geoscience, Delft, 1998.

Huntington, T. G.: Evidence for Intensification of the Global Water Cycle: Review and Synthesis, Journal of Hydrology, 319, 83–95, https://doi.org/10.1016/j.jhydrol.2005.07.003, 2006.

Jacobs, C., Elbers, J., Brolsma, R., Hartogensis, O., Moors, E., Rodríguez-Carretero Márquez, M. T., and van Hove, B.: Assessment of Evaporative Water Loss from Dutch Cities, Building and Environment, 83, 27–38, https://doi.org/10.1016/j.buildenv.2014.07.005, 2015.

15 Jung, M., Reichstein, M., Ciais, P., Seneviratne, S. I., Sheffield, J., Goulden, M. L., Bonan, G., Cescatti, A., Chen, J., de Jeu, R., Dolman, A. J., Eugster, W., Gerten, D., Gianelle, D., Gobron, N., Heinke, J., Kimball, J., Law, B. E., Montagnani, L., Mu, Q., Mueller, B., Oleson, K., Papale, D., Richardson, A. D., Roupsard, O., Running, S., Tomelleri, E., Viovy, N., Weber, U., Williams, C., Wood, E., Zaehle, S., and Zhang, K.: Recent Decline in the Global Land Evapotranspiration Trend Due to Limited Moisture Supply, Nature, 467, 951–954, https://doi.org/10.1038/nature09396, 2010.

20 Keijman, J. Q. and Koopmans, R. W. R.: A Comparison of Several Methods of Estimating the Evaporation of Lake Flevo, International Association of Hydrological Sciences Publ., 109, 225–232, 1973.

Kitaigorodskii, S. A. and Miropolskii, Y. Z.: On the Theory of the Open Ocean Active Layer, Izv. Atmos. Oceanic Phys., 6, 97–102, 1970.

Kleidon, A. and Renner, M.: An Explanation for the Different Climate Sensitivities of Land and Ocean Surfaces Based on the Diurnal Cycle, Earth System Dynamics, 8, 849–864, https://doi.org/https://doi.org/10.5194/esd-8-849-2017, 2017.

25 La, Z.: Quantifying Evaporation and Its Decadal Change for Lake Nam Co, Central Tibetan Plateau, AGU Fall Meeting Abstracts, 23, GC23L–1256, 2015.

Lenters, J. D., Kratz, T. K., and Bowser, C. J.: Effects of Climate Variability on Lake Evaporation: Results from a Long-Term Energy Budget Study of Sparkling Lake, Northern Wisconsin (USA), Journal of Hydrology, 308, 168–195, https://doi.org/10.1016/j.jhydrol.2004.10.028, 2005.

30 Makkink, G. F.: Testing the Penman Formula by Means of Lysimeters, Journal of the Institution of Water Engineers, 11, 277–288, 1957.

Melsen, L. A., Addor, N., Mizukami, N., Newman, A. J., Torfs, P. J. J. F., Clark, M. P., Uijlenhoet, R., and Teuling, A. J.: Mapping (Dis)Agreement in Hydrologic Projections, Hydrology and Earth System Sciences, 22, 1775–1791, https://doi.org/10.5194/hess-22-1775-2018, 2018.

Middelkoop, H., Daamen, K., Gellens, D., Grabs, W., Kwadijk, J. C. J., Lang, H., Schulla, J., and Wilke, K.: Impact of Climate Change on
35 Hydrological Regimes and Water Resources Management in the Rhine Basin., 49, 105–128, 2001.

Mironov, D. V.: Parameterization of Lakes in Numerical Weather Prediction – Description of a Lake Model, COSMO Technical Report No. 11, Deutscher Wetterdienst, Offenback am Main, Germany, 2008.

Moene, A. F. and van Dam, J. C.: Transport in the Atmosphere-Vegetation-Soil Continuum, Cambridge University Press, 2014.

23

Moors, E. J.: Water Use of Forests in The Netherlands, PhD Thesis, Vrije Universiteit Amsterdam, Amsterdam, 2012.

Nordbo, A., Launiainen, S., Mammarella, I., Leppäranta, M., Huotari, J., Ojala, A., and Vesala, T.: Long-Term Energy Flux Measurements
   and Energy Balance over a Small Boreal Lake Using Eddy Covariance Technique, Journal of Geophysical Research: Atmospheres, 116,
   https://doi.org/10.1029/2010JD014542, 2011.

5 Oki, T. and Kanae, S.: Global Hydrological Cycles and World Water Resources, Science, 313, 1068–1072,
   https://doi.org/10.1126/science.1128845, 2006.

Penman, H. L.: Natural Evaporation from Open Water, Bare Soil and Grass, Proceedings of the Royal Society of London. Series A, Mathe-
   matical and Physical Sciences, 193, 120–145, 1948.

Priestley, C. H. B. and Taylor, R. J.: On the Assessment of Surface Heat Flux and Evaporation Using Large-Scale Parameters, Monthly
10   Weather Review, 100, 81–92, https://doi.org/10.1175/1520-0493(1972)100<0081:OTAOSH>2.3.CO;2, 1972.

Renner, M., Brenner, C., Mallick, K., Wizemann, H.-D., Conte, L., Trebs, I., Wei, J., Wulfmeyer, V., Karsten, S., and Kleidon, A.: Under-
   standing Model Biases in the Diurnal Cycle of Evapotranspiration: A Case Study in Luxembourg, Hydrology and Earth System Sciences
   Discussions, pp. 1–36, https://doi.org/10.5194/hess-2018-310, 2018.

Rosenberry, D. O., Winter, T. C., Buso, D. C., and Likens, G. E.: Comparison of 15 Evaporation Methods Applied to a Small Mountain Lake
15   in the Northeastern USA, Journal of Hydrology, 340, 149–166, https://doi.org/10.1016/j.jhydrol.2007.03.018, 2007.

Solcerova, A., van de Ven, F., and van de Giesen, N.: Nighttime Cooling of an Urban Pond, Frontiers in Earth Science, 7,
   https://doi.org/10.3389/feart.2019.00156, 2019.

Tanny, J., Cohen, S., Assouline, S., Lange, F., Grava, A., Berger, D., Teltch, B., and Parlange, M. B.: Evaporation from a Small Water
   Reservoir: Direct Measurements and Estimates, Journal of Hydrology, 351, 218–229, https://doi.org/10.1016/j.jhydrol.2007.12.012, 2008.

20 Teuling, A. J.: A Forest Evapotranspiration Paradox Investigated Using Lysimeter Data, Vadose Zone Journal, 17, 0,
   https://doi.org/10.2136/vzj2017.01.0031, 2018.

Trenberth, K. E., Dai, A., van der Schrier, G., Jones, P. D., Barichivich, J., Briffa, K. R., and Sheffield, J.: Global Warming and Changes in
   Drought, Nature Climate Change, 4, 17–22, https://doi.org/10.1038/nclimate2067, 2014.

van Emmerik, T., Rimmer, A., Lechinsky, Y., Wenker, K., Nussboim, S., and van de Giesen, N.: Measuring Heat Balance Residual at Lake
25   Surface Using Distributed Temperature Sensing: Measuring Lake Heat Balance Residual Using DTS, Limnology and Oceanography:
   Methods, 11, 79–90, https://doi.org/10.4319/lom.2013.11.79, 2013.

van Meijgaard, E., van Ulft, L. H., van de Berg, W. J., Bosveld, F. C., van den Hurk, B. J. J. M., Lenderink, G., and Siebesma, A. P.: The
   KNMI Regional Atmospheric Climate Model RACMO, Version 2.1, Technical Report TR-302, KNMI, De Bilt, 2008.

Venäläinen, A., Frech, M., Heikinheimo, M., and Grelle, A.: Comparison of Latent and Sensible Heat Fluxes over Boreal Lakes
30   with Concurrent Fluxes over a Forest: Implications for Regional Averaging, Agricultural and Forest Meteorology, 98-99, 535–546,
   https://doi.org/10.1016/S0168-1923(99)00100-8, 1999.

Verburg, P. and Hecky, R. E.: The Physics of the Warming of Lake Tanganyika by Climate Change, Limnology and Oceanography, 54,
   2418–2430, https://doi.org/10.4319/lo.2009.54.6_part_2.2418, 2009.

Vermeulen, M. H., Kruijt, B. J., Hickler, T., and Kabat, P.: Modelling Short-Term Variability in Carbon and Water Exchange in a Temperate
35   Scots Pine Forest, Earth System Dynamics, 6, 485–503, https://doi.org/https://doi.org/10.5194/esd-6-485-2015, 2015.

Vörösmarty, C. J.: Global Water Resources: Vulnerability from Climate Change and Population Growth, Science, 289, 284–288,
   https://doi.org/10.1126/science.289.5477.284, 2000.

Wieringa, J.: Metingen van het Flevo-1967 verdampingsonderzoek., Technisch rapport, p. 9, 2019.

Zhan, S., Song, C., Wang, J., Sheng, Y., and Quan, J.: A Global Assessment of Terrestrial Evapotranspiration Increase Due to Surface Water Area Change, Earth's Future, 7, 266–282, https://doi.org/10.1029/2018EF001066, 2019.

Appendix A

Table A1. Evaporation methods further explained

(a) Information about the evaporation methods

Method	Category	Equation	Input data	Assumptions
Penman	Combination	$\lambda E = \frac{s}{s+\gamma} Q_n + \frac{\gamma}{s+\gamma} E_a$	T_{air}, R_n, u, RH, P	1) closed energy balance at water surface 2) e_{sat} at surface decreases linearly to e_{sat} at observation height 3) r_a can be estimated by a wind function
De Bruin -	Combination	$\lambda E = \alpha_{BK} \frac{s}{s+\gamma} (R_n - G) + \beta_{BK}$	T_{air}, R_n	1) constant proportionality between radiation and aerodynamic term
Keijman				2) aerodynamic term can be described by a constant, assuming no explict wind effects 3) Heat storage often assumed to be negligible
Makkink	Energy	$\lambda E = 0.65 \frac{s}{s+\gamma} K_{in}$	T_{air}, K_{in}	1) heat storage is negligible in relation to R_n 2) R_n is half of K_{in} 3) wind speed does not need to be accounted for explicitly
Granger &	Wind	$E = a * u$	u, RH, x_{shore}, ΔT, Δe	1) No relation between E_{water} and R_n at hourly timescales
Hedstrom		$a = f(\Delta T, \Delta e, X)$		2) Atmospheric stability can be described by land-lake temperature contrast 3) Non-linear over-all relation between E_{water} and u is approximated by linear relation
Hargreaves	Temperature	$ET_{ref} = 0.0023 R_a (TC + 17.8) TR^{0.50}$	T_{air}, R_a	1) K_{in} can be approximated using the extraterrestrial radiation 2) Cloudiness is represented using the temperature range 3) No heat storage since method is developed for land surfaces
FLake	physical-oriented	$\lambda E = -(q_z - q_s) \frac{u_* k}{Sc_n} \frac{L_v \rho}{(ln(\frac{z}{z_0}) + \psi_q(z/L))}$	T_{air}, K_{in}, u, RH, cloudiness, $d_{lake}, x_{fetch}, \epsilon$	1) Top layer of lake is assumed to be well mixed 2) Thermocline in bottom layer is described with concept of self-similarity of temperature profile

(b) Variables and constants needed as input data for the methods

Variable/Constant	Unit
α_{BK} = 1.1 = De Bruin-Keijman emperically derived constant	[–]
β_{BK} = 10 = De Bruin-Keijman empirically derived constant	[W m^{-2}]
γ = psychrometric 'constant'	[kPa °C^{-1}]
Δe = Horizontal vapour pressure gradient, lake-land	[°C]
ΔT = Horizontal temperature gradient, land-lake	[°C]
ϵ = Light extinxtion coefficient	[m^{-1}]
λE = latent heat flux	[W m^{-2}]
ρ = Air density	[kg m^{-3}]
ψ_q = Dimensionless function accounting for static stability in the surface layer	[–]
d_{lake} = Lake depth	[m]
E_a = drying power of air, representing water vapour transport capacity of the atmosphere	[W m^{-2}]
G = water/ground heat flux	[W m^{-2}]
k = Von Karman constant	[–]
K_{in} = incoming shortwave radiation	[W m^{-2}]
L = Obukhov length	[m]
L_v = Latent heat of vaporization	[kJ kg^{-1}]
P = Air pressure	[kPa]
Q_n = available energy	[W m^{-2}]
q_s = Saturated specific humidity at the surface	[–]
q_z = Air specific humidity at height z	[–]
RH = Relative Humidity	[–]
R_a = Extraterrestrial radiation	[MJ m^{-2} d^{-1}]
R_n = Net radiation	[W m^{-2}]
s = slope of the saturated vapour pressure curve	[kPa °C^{-1}]
Sc_n = Schmidt number	[–]
T_{air} = Temperature	[°C]
TC = Temperature	[°C]
TR = Temperature range	[°C]
u = Wind speed	[m s^{-1}]
u_* = Friction velocity	[m s^{-1}]
x_{shore} = Distance to the shore	[m]
x_{fetch} = Fetch distance	[m]
z = Height of measurements of temperature and humidity	[m]
z_0 = Roughness length for specific humidity	[m]